

# Cation-Specific Effects on Enzymatic Catalysis Driven by Interactions at the Tunnel Mouth

Veronika Štěpánková,<sup>†,‡</sup> Jana Paterová,<sup>§</sup> Jiří Damborský,<sup>†,‡</sup> Pavel Jungwirth,<sup>§</sup> Radka Chaloupková,<sup>\*,†</sup> and Jan Heyda<sup>\*,§,¶</sup>

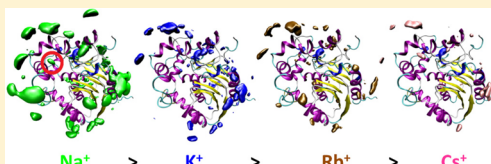
<sup>†</sup> Loschmidt Laboratories, Department of Experimental Biology and Research Centre for Toxic Compounds in the Environment, Masaryk University, Kamenice 5/A13, 625 00 Brno, Czech Republic

<sup>‡</sup> International Clinical Research Center, St. Anne's University Hospital Brno, Pekarska 53, 656 91 Brno, Czech Republic

<sup>§</sup> Institute of Organic Chemistry and Biochemistry, Academy of Sciences of the Czech Republic, Flemingovo nám. 2, 166 10 Prague 6, Czech Republic

## S Supporting Information

**ABSTRACT:** Cationic specificity which follows the Hofmeister series has been established for the catalytic efficiency of haloalkane dehalogenase LinB by a combination of molecular dynamics simulations and enzyme kinetic experiments. Simulations provided a detailed molecular picture of cation interactions with negatively charged residues on the protein surface, particularly at the tunnel mouth leading to the enzyme active site. On the basis of the binding affinities, cations were ordered as  $\text{Na}^+ > \text{K}^+ > \text{Rb}^+ > \text{Cs}^+$ .



In agreement with this result, a steady-state kinetic analysis disclosed that the smaller alkali cations influence formation and productivity of enzyme–substrate complexes more efficiently than the larger ones. A subsequent systematic investigation of two LinB mutants with engineered charge in the cation-binding site revealed that the observed cation affinities are enhanced by increasing the number of negatively charged residues at the tunnel mouth, and vice versa, reduced by decreasing this number. However, the cation-specific effects are overwhelmed by strong electrostatic interactions in the former case. Interestingly, the substrate inhibition of the mutant LinB L177D in the presence of chloride salts was 7 times lower than that of LinB wild type in glycine buffer. Our work provides new insight into the mechanisms of specific cation effects on enzyme activity and suggests a potential strategy for suppression of substrate inhibition by the combination of protein and medium engineering.

## INTRODUCTION

Ion-specific effects play an important role in biochemical and biophysical processes. Biological systems usually undergo a significant stress when salt concentrations are varied or one ion is replaced by another.<sup>1</sup> Traditionally, ions have been ordered in the so-called Hofmeister series according to their ability to salt out proteins.<sup>2,3</sup> However, many other processes, including enzymatic activity and thermal stability, also exhibit ion specificity.<sup>4</sup> The emerging view, based on molecular simulations and laboratory experiments, is that ion effects are actually a complex phenomenon involving local interactions between ions and functional groups at the protein surface<sup>5</sup> as well as ion–ion interactions in the solution.<sup>6</sup> Ordering cations and anions into separate series proved to be a simplification, which may not be always justified.<sup>7,8</sup> Nevertheless, in many cases, formulating Hofmeister series provides a reasonable starting point in attempts to understand the fundamental molecular mechanisms.

The effects of anions on protein solubility and stability are typically stronger than those of cations, at least monovalent ones, while the enzyme activity can be significantly affected by both anions and cations.<sup>9,10</sup> After all, a basic asymmetry in biology which propels many physiological processes is that of the intracellular potassium versus extracellular sodium concen-

trations. From the interaction point of view, these two monovalent cations differ only slightly in size, but the consequences for cellular mechanisms are dramatic.<sup>11</sup> At the level of enzymatic activity, the previously observed differences between effects of  $\text{Na}^+$  versus  $\text{K}^+$  were more subtle, but still important.<sup>12</sup> It was shown that replacing sodium by potassium enhances significantly the enzymatic activity of the HIV protease.<sup>13,14</sup> Most recently, the activity of HIV protease was studied in the presence of four alkali cations,  $\text{Li}^+$ ,  $\text{Na}^+$ ,  $\text{K}^+$ , and  $\text{Cs}^+$ , and it was found out that the alkali cations can be essentially systematized into a Hofmeister-like series.<sup>15</sup> The likely origin of this ordering is the fact that smaller alkali cations interact more strongly than the bigger ones with the anionic carboxylic groups of the glutamate and aspartate side chains. Of particular importance could be a pair of aspartates at the entrance to the active site where more strongly bound cations may hamper the binding of a mostly hydrophobic substrate.<sup>14,15</sup> The strength of this effect is, however, not yet unequivocally established.<sup>16</sup>

**Received:** February 11, 2013

**Revised:** April 23, 2013

**Published:** April 29, 2013

Haloalkane dehalogenases (EC 3.8.1.5, HLDs) are  $\alpha/\beta$ -hydrolases which cleave the carbon–halogen bonds, and thus convert halogenated compounds to the corresponding alcohols, halides, and protons.<sup>17</sup> The reaction accomplished by a catalytic pentad—a nucleophile (Asp), a general base (His), a catalytic acid (Asp/Glu), and halide-stabilizing residues (Trp and Trp/Asn)—proceeds by the nucleophilic attack of the carboxylate oxygen of an aspartate group on the carbon atom of the substrate, yielding displacement of the halogen and the formation of a covalent alkyl–enzyme intermediate. Subsequently, alkyl–enzyme intermediate is hydrolyzed by a water molecule activated by a catalytic base (Figure 1). The

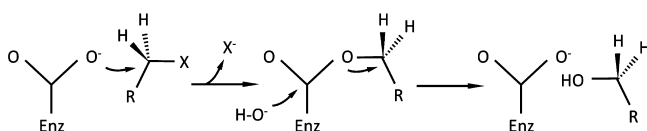


**Figure 1.** General scheme of the reaction mechanism of haloalkane dehalogenases.

charge developed on the imidazole ring of a catalytic base during the hydrolytic reaction is stabilized by a catalytic acid. The catalytic pentad is situated in a deeply buried, predominantly hydrophobic active-site cavity connected to the bulk solvent by an access tunnel.<sup>18,19</sup> The high importance of the tunnel residues for enzymatic activity was previously established by site-directed mutagenesis and directed evolution experiments, showing that both enzyme activity and stability can be improved by modifying access pathways leading to the enzyme active site.<sup>20,21</sup>

The aim of this study was to find out how individual alkali cations interact with the enzyme surface, and how this interaction affects the enzymatic activity. The HLD LinB from *Sphingobium japonicum* UT26<sup>22</sup> was chosen as a model system for our combined computational and experimental study. On the computational side, the wild type (wt) LinB in the presence of 0.5 M solutions of NaCl, KCl, RbCl, or CsCl was subjected to molecular dynamics simulations. The generated trajectories provided spatial distributions of the four alkali cations at the enzyme surface. The site located around the tunnel mouth, which serves for substrates and products as a gateway from the active site, has been identified as the key region for specific ion effects on the activity of LinB. Based on the simulation results, two LinB mutants differing in cationic binding at the tunnel mouth were constructed. Together with the wt enzyme, they were functionally characterized by steady-state kinetics in aqueous solutions of alkali chloride salts. This combined study contributes toward understanding cationic Hofmeister effects on HLDs at a molecular level.

## METHODS

**Computational Methods. Molecular Dynamics Simulations.** LinB wt in its crystal structure geometry (PDB accession no. 1MJS)<sup>23</sup> was solvated in ~11 100 SPC/E water molecules. This includes both water molecules from the crystal structure and additional randomly placed bulk water molecules. The uncertainty about the protonation state of the catalytic histidine (H272), which may change during the enzymatic cycle, led us to independent investigation of two scenarios: (i) histidine doubly protonated at both N<sub>e</sub> and N<sub>δ</sub> atoms (i.e., charged) and (ii) histidine singly protonated at the N<sub>δ</sub> atom

(i.e., neutral). The total charge of the investigated enzyme was consequently −10 e in the case (i) and −11 e in the case (ii). This charge was compensated by counterions (cations), which were of the same chemical nature as those of the added 0.5 M salt (realized by 100 alkali cations and 100 chloride anions that replaced randomly selected water molecules in the bulk region). All results presented in the main text assume a doubly protonated catalytic histidine; corresponding results for singly protonated catalytic histidine are given in the Supporting Information. The parametrization of Na<sup>+</sup>, K<sup>+</sup>, Rb<sup>+</sup>, and Cs<sup>+</sup> cations (with Rb<sup>+</sup> σ-parameter interpolated between those of K<sup>+</sup> and Cs<sup>+</sup>) and Cl<sup>−</sup> was the same as in our earlier studies,<sup>14,24</sup> which proved to be a reliable choice in combination with the ff03 protein force field<sup>25</sup> and the SPC/E water model.<sup>26</sup> In the case of LinB mutants—LinB D147N, LinB L177D, and LinB D147N-L177D—the computations were started from the final conformation of LinB wt, since the crystal structures of these mutants are not known. Systems with mutants were subjects of an identical simulation protocol as the LinB wt systems. The exact compositions of all systems are summarized in Table S1 in the Supporting Information.

Calculations were carried out using the Amber 11 program package<sup>27</sup> according to the simulation protocol used in our previous protein studies.<sup>14,28</sup> Potential energy of the system was first minimized with constrained positions of protein atoms using the steepest descent method in order to avoid unfavorable close contacts. The system was then slowly heated up to 300 K with volume held fixed and, subsequently, pressure coupling was employed to reach the equilibrium density. Equilibration lasted for 2 ns and the data were collected from the subsequent 100 ns production runs. All bonds involving hydrogen atoms were constrained using the SHAKE algorithm, allowing 2 fs time step.<sup>29</sup> The short-range nonbonded interactions were cut off at 9 Å and smooth particle mesh Ewald (PME) method accounted for the long-range electrostatics.<sup>30</sup> The Berendsen pressure and temperature coupling schemes (with coupling frequency of 1 ps<sup>−1</sup>) were introduced.<sup>31</sup>

**Analysis of the Simulation Data.** In this study, a detailed description of ionic distributions at global as well as local scales was essential, since the key region for specific ion effects on the activity of LinB is likely located around the tunnel leading to the active site.<sup>23</sup> Thus, in addition to the spatial distributions of ions at the enzyme surface as a whole, the most relevant sites around the tunnel mouth were investigated separately in terms of radial and proximal distribution functions. Before the ionic distributions were constructed, the simulated data were first analyzed in terms of protein stability (i.e., root-mean-square deviation from the initial crystal structure, radius of gyration, and preservation of secondary structure elements) and active site stability (i.e., key distances that are preserved in vast majority of LinB crystal structures). These properties were monitored on the whole 100 ns simulation time scale in order to verify that the simulations provide reasonable conformations and no artificially distorted structures (see Supporting Information for details).

The spatial distribution functions were then calculated as the ratios of the local (spatially resolved) density and bulk density of ions, reaching unity far from the protein. Close to the protein surface this function can exhibit sharp peaks. In these cases, the spatial regions in the vicinity of the surface, where ions occur with significantly enhanced probabilities, were visualized by employing isocontours, i.e., cuts through these peaks. It is

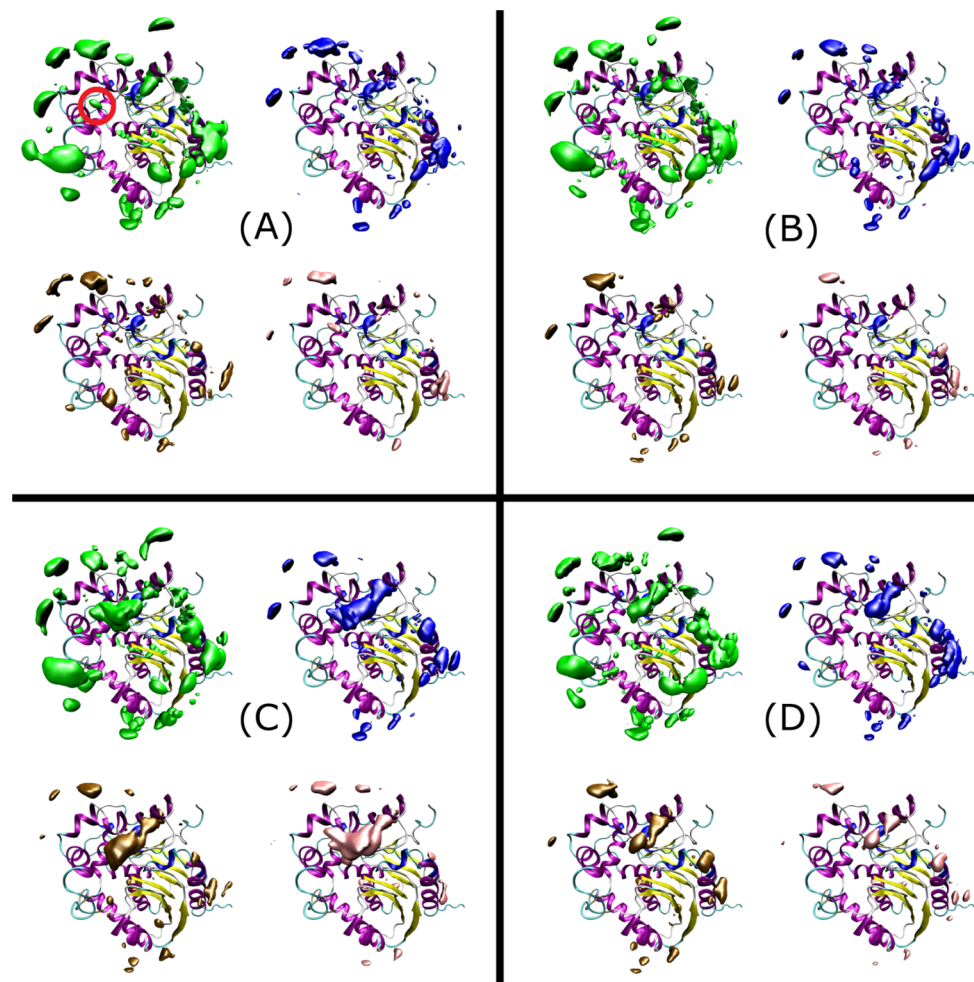


**Figure 2.** Spatial distribution function of alkali cations (color coding:  $\text{Na}^+$  green,  $\text{K}^+$  blue,  $\text{Rb}^+$  brown, and  $\text{Cs}^+$  pink) around the protein surface. The black border lines separate (A) LinB wt, (B) LinB D147N, (C) LinB L177D, and (D) LinB D147N-L177D. The probability clouds are shown at the level of 5 times the average bulk cation density. The enzyme is oriented such that the tunnel mouth is situated in the middle of the picture (red circled).

important to note that by integrating the spatial distribution function over the two angular coordinates the standard radial distribution function can be obtained. In order to reduce noise, the spatial distribution functions were acquired assuming Gaussian shapes of ions or atoms with the half-width of  $1 \text{ \AA}^{32}$ .

**Experimental Methods. Site-Directed Mutagenesis.** Mutant recombinant genes for two single-point LinB mutants (*linB\_D147N* and *linB\_L177D*) and a doublepoint mutant (*linB\_D147N-L177D*) were constructed according to the protocol for QuikChange Site-Directed Mutagenesis Kit (Stratagene). The oligonucleotides used to introduce mutations in positions 147 and 177 were as follows: D147N (5'-CCGAACAGAATCGCGATCTG-3') and L177D (5'-CTCCCCGGGACATCCTGCGC-3') plus the reverse complementary ones (substitutions are underlined). Plasmids pUC18 with the gene *linB* or mutant recombinant gene *linB\_L177D* were used as templates for single-point mutants and double-point mutant, respectively. Mutant recombinant genes were subcloned into a pAQN vector<sup>23</sup> using *Eco*RI and *Hind*III restriction endonucleases, and a T4 DNA ligase (New England BioLabs). The nucleotide sequences were determined commercially (Macrogen).

**Protein Expression and Purification.** The His-tagged enzymes were overexpressed in *Escherichia coli* BL21 cells

using a previously described method.<sup>20,33</sup> Proteins were purified on a Ni-NTA Superflow Cartridge (Qiagen). His-tagged enzymes were bound to the resin in an equilibrating buffer (20 mM potassium phosphate buffer, pH 7.5 containing 0.5 M sodium chloride and 10 mM imidazole). Unbound and weakly bound proteins were washed out. His-tagged enzymes were eluted by a buffer containing 300 mM imidazole. The active fractions were pooled and dialyzed overnight against 50 mM potassium phosphate buffer (pH 7.5) and then stored at 4 °C. Protein concentration was determined by a Bradford reagent (Sigma-Aldrich). Purity of purified proteins was checked by SDS-PAGE.

**Circular Dichroism Spectroscopy.** Circular dichroism (CD) spectra of enzymes were determined at 37 °C using the Jasco J-810 spectropolarimeter equipped with the Peltier thermostat (Jasco). Data were collected from 200 to 260, at 100 nm/min, 1 s response time and 2 nm bandwidth. Spectra were recorded in a 0.1 cm quartz cuvette containing 0.25 mg/mL enzyme in 50 mM phosphate buffer (pH 7.5) and 0.5 M chloride salts. Each spectrum shown is the average of five scans and baseline corrected. CD spectra were expressed as the mean residue ellipticity,  $\theta_{\text{MRE}}$  calculated according to eq 1:

$$\theta_{\text{MRE}} = (\theta_{\text{obs}} M_w \cdot 100) / (ncl) \quad (1)$$

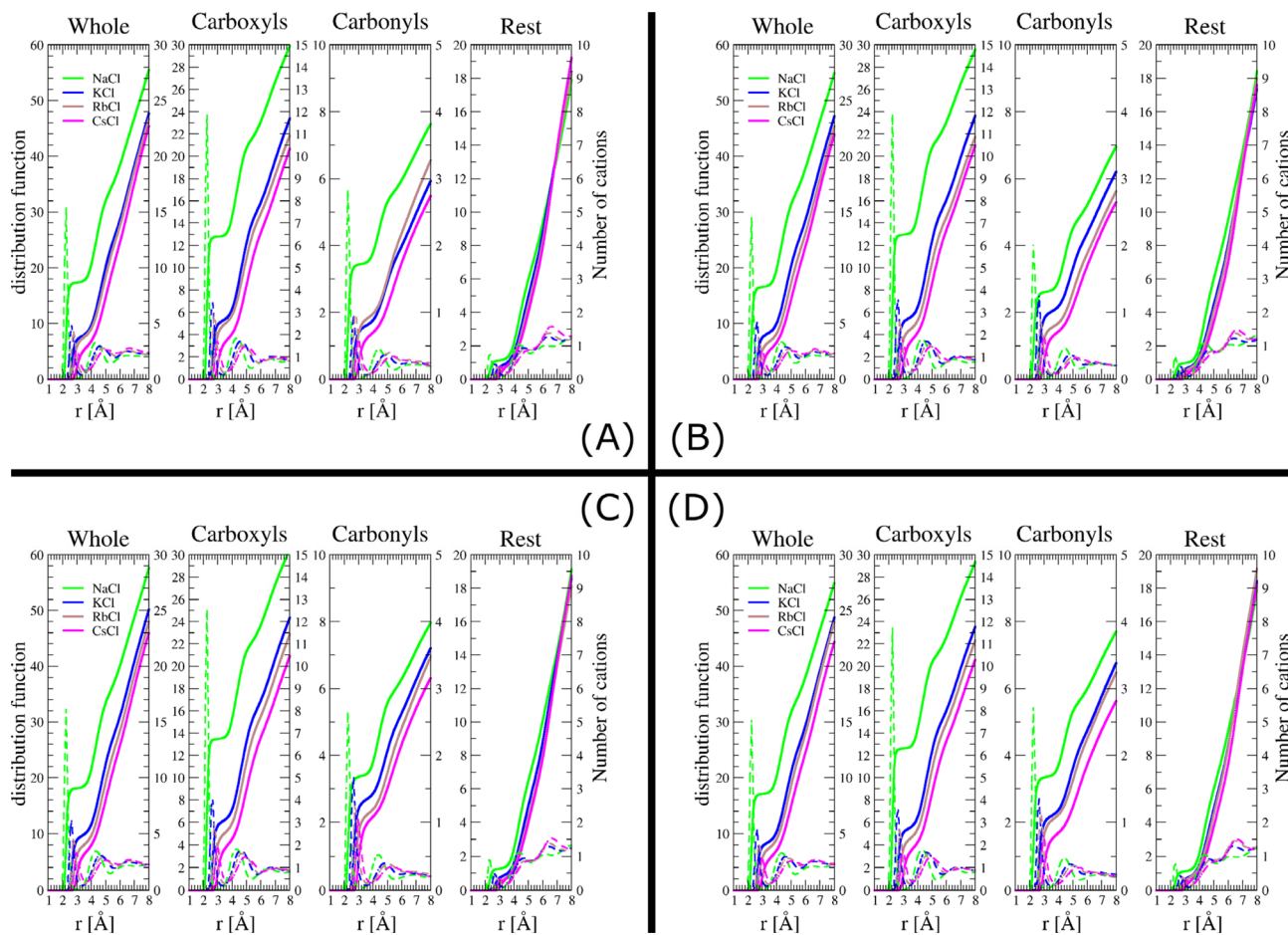


**Figure 3.** Proximal running coordination numbers (full line, right axis) and their derivatives, distribution functions, (dashed line, left axis) of cations from the protein surface, which is further divided into carboxyl groups, carbonyl groups, and the rest. The black border lines separate (A) LinB wt, (B) LinB D147N, (C) LinB L177D, and (D) LinB D147N-L177D.

where  $\theta_{\text{obs}}$  is the observed ellipticity in degrees,  $M_w$  is the protein molecular weight,  $n$  is number of residues,  $l$  is cell path length,  $c$  is protein concentration, and the factor 100 originates from the conversion of the molecular weight to mg/dmol.

**Isothermal Titration Calorimetry.** Substrate to product conversion by the action of enzymes was carried out using VP-ITC isothermal titration microcalorimeter (MicroCal) by a single injection method. The substrate 1-iodohexane was dissolved in 100 mM glycine buffer (pH 8.6) containing an appropriate molar volume of chloride salts and equilibrated at 37 °C in the sample cell (1.4 mL). The reaction was initiated by the injection of 10 μL of 0.5 mg/mL enzyme solution dialyzed overnight against the same solution as used for dissolving the substrate. Heat flow ( $\mu\text{cal s}^{-1}$ ) was recorded as a function of time. The reaction rate was calculated according to the eq 2.

$$\frac{dQ}{dt} = -\Delta H V \frac{d[S]}{dt} \quad (2)$$

In this equation,  $V$  is the volume of the sample cell,  $[S]$  is the substrate concentration, and  $\Delta H$  is the enthalpy of the conversion of substrate to product. This was determined experimentally by titration of the substrate into the sample cell containing the enzyme. The evaluated rate of substrate depletion and corresponding substrate concentration were fitted by nonlinear regression to kinetic models by using software Origin 6.1 (OriginLab).

## RESULTS AND DISCUSSION

**Computation.** After performing MD simulations, we first analyzed the stability of LinB wt in various salt solutions (0.5 M NaCl, KCl, RbCl, and CsCl) in terms of root-mean-square deviation from the crystal structure (rmsd), radius of gyration ( $R_g$ ), and secondary structure elements. In all investigated systems, these parameters showed that the LinB wt structure does not deviate significantly from the initial crystal structure on the ~100 ns time scale (for details see Supporting Information).

In recent studies on different proteins,<sup>14,34</sup> we demonstrated the usefulness of mapping positions of highest occurrence of ions in terms of the spatial distribution function and to divide the protein surface into distinct functional areas, to which the ionic affinity is quantified in terms of proximal distribution functions and running coordination numbers. Similarly, the overall averaged preferences of cations for negatively charged carboxyl groups, backbone carbonyl groups, and the rest of the LinB wt surface were displayed in this study. Figure 2 demonstrates that sodium possesses the strongest interaction with the protein surface among the investigated alkali cations. Sodium binding to the sites placed all over the -10 e charged LinB wt surface strongly correlates with the distribution of negatively charged aspartate and glutamate residues. Keeping the same isolevel, we show in Figure 2 that the potassium, rubidium, and cesium cations interact at the same sites as

sodium, albeit more weakly. The clouds of rubidium are slightly weaker than those of potassium and most of the cesium clouds are barely detectable at the same isolevel. To further support the claim about the equivalence of the cation-binding sites, the same spatial distribution function but with unequal isovalues, so that the clouds were roughly of the same size, were displayed (see Figure S1 in the Supporting Information). These spatial distribution functions capture graphically very well the inhomogeneous affinities of cations toward the LinB wt surface. However, due to the 3D nature of this variable, only cuts at certain isolevels can be shown, presenting mainly qualitative behavior and changes. For a more quantitative evaluation of the cationic affinities to the enzyme surface, the proximal coordination numbers were evaluated. Within this analysis, each ion was at each snapshot assigned to the closest region at the protein surface. Results presented in Figure 3 show again that sodium binds the strongest to LinB wt and that its overall affinity gains mainly from the negatively charged carboxyl groups of aspartates and glutamates and, to lesser extent, also from the surface exposed carbonyl groups of the backbone and side chains of asparagine or glutamine. The remaining part of the surface did not exhibit much of ion affinity or specificity. The cation affinity to carboxyl and carbonyl groups decreased with the increasing size of the cation. Already potassium binds significantly weaker than sodium, while the difference between potassium and rubidium is only modest, with cesium distinctly exhibiting the smallest affinity for LinB wt. Finally, when compared to simulations of LinB with neutral H272 in the active site (see Supporting Information) the results are very similar, the magnitude of the cationic effects being only slightly heightened by the increase of the negative charge of the enzyme via deprotonating the histidine residue.

Although the cation binding sites were found all around the LinB wt surface, the previous study on LinB points to the fact that changes in cationic affinities around the tunnel mouth should be the most important.<sup>20</sup> Therefore, seven regions near the tunnel mouth where ions occur with enhanced probability were denoted as hotspots (Figure 4, and Table S2 in the Supporting Information). Among the identified hotspots, that

labeled as S1 located right above the tunnel mouth was recognized as the most likely candidate to exhibit a significant effect on enzymatic activity. To explore and quantify the cationic affinities at this region into more detail, we employed three complementary methods: (i) calculation of radial distribution functions (RDFs) to the S1-forming residues (Figure 5), (ii) calculation of the proximal running coordination number from three  $C_\alpha$  atoms that form corners of the tunnel mouth (Figure 6), and (iii) determination of the numbers of cations along the truncated-cone axis, which begins at the active site and protrudes along the tunnel toward the protein surface (Figure S6 in the Supporting Information). The results essentially support the cationic ordering found for global cationic affinities; however, the coordination numbers (i.e.,  $r^2$ -weighted integrals of the RDFs) to the carboxyl group of D147 are rather similar for all four investigated cations (Table S5 in the Supporting Information).

To further analyze the cationic binding at the tunnel mouth, two single-point mutants (LinB D147N and LinB L177D) and a double-point mutant (LinB D147N-L177D) that differ in the charge at the hotspot S1 were examined. The calculation of rmsd,  $R_g$ , and secondary structure elements of all studied mutants confirmed their conformational stability in the presence of the investigated alkali chloride salts (Figures S8–S10 in the Supporting Information). The overall spatial distribution functions, the proximal running coordination numbers, and distribution functions for LinB mutants differ very little from those for LinB wt (Figures 2 and 3). Both D147N and L177D mutations are located at the tunnel mouth and affect only the cationic clouds located nearby. Figure 2B shows that the reduced charge at the tunnel mouth of LinB D147N led to disappearance of the corresponding cationic cloud right above the tunnel mouth (circled position in Figure 4), suggesting a vanishing affinity of all cations to this region (Figure 5B). All other cationic clouds remained at their original positions and were of the very same magnitude as for the LinB wt. In contrast, the additional negative residue introduced to the tunnel mouth of LinB L177D caused an enhancement of the cationic cloud that disappeared during the previous mutation (Figure 2C). Interestingly, this cloud was more pronounced for larger alkali cations than sodium, implying that L177D mutation boosted cation affinity, albeit with a weaker cationic specificity (Figure 5C). In the case of the double mutant LinB D147N-L177D, which carries both the above mutations, the mutation D147N was found to be more important than L177D, and thus they were not fully compensated locally (Figures 2D and 5D). At larger distances, however, the effects of these two mutations tend to compensate each other, as seen from G176 and Q146 RDFs, explaining why the spatial distribution function copies that of the LinB wt.

Due to the flexibility of the side chains, the numbers of cations within a spatially fixed region in the vicinity of the tunnel mouth, corresponding to the S1 hotspot, were additionally counted (Figure 6). For LinB wt,  $\text{Na}^+$  binding was the strongest, that of  $\text{Cs}^+$  was the weakest, while  $\text{Rb}^+$  and  $\text{K}^+$  signals were in between, close to each other. As observed already from RDFs, mutations changing the charge at the tunnel mouth resulted in corresponding changes in the strengths of the cationic binding. Additionally, in accord with RDFs observation, ion specificity is preserved for the D147N mutant, while it all but vanishes for the L177D mutant. Moreover, the numbers of cations within a truncated cone that starts in the LinB active site and protrudes toward the tunnel

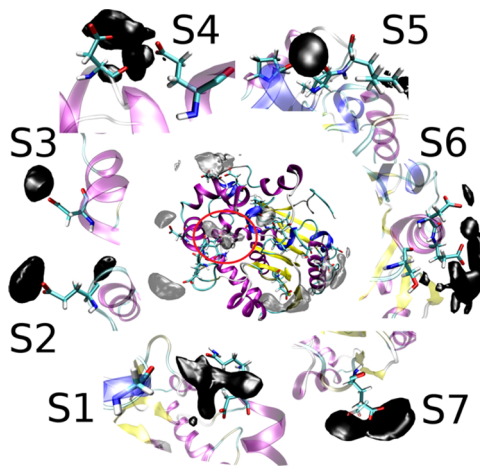


**Figure 4.** Visualization of the tunnel mouth in LinB wt as mapped by  $\text{Na}^+$  funnel-like spatial density distribution in the hot-spot S1 (red circled in the central picture). The most occupied regions (transparent black clouds) in the close vicinity of the tunnel mouth are visualized in the central LinB figure. The hot-spot regions S1–S7 are magnified around.

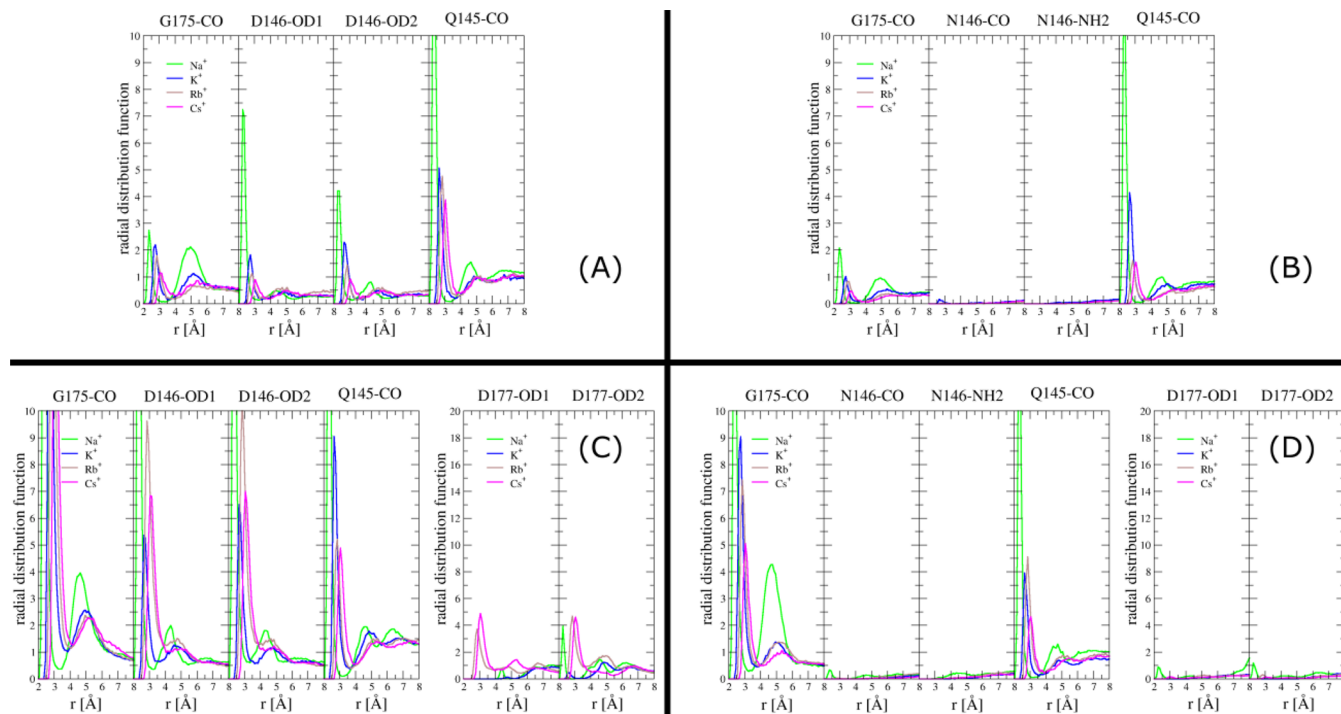


**Figure 5.** Radial distribution functions (RDFs) of cations to the S1 hot-spot region, formed by G176, D147, and Q146 residues. The black border lines separate (A) LinB wt, (B) LinB D147N, (C) LinB L177D, and (D) LinB D147N-L177D. When the mutation L177D was present, we added the RDFs to the new carboxyl group at the tunnel mouth (plots for two D177 carboxyl oxygens).

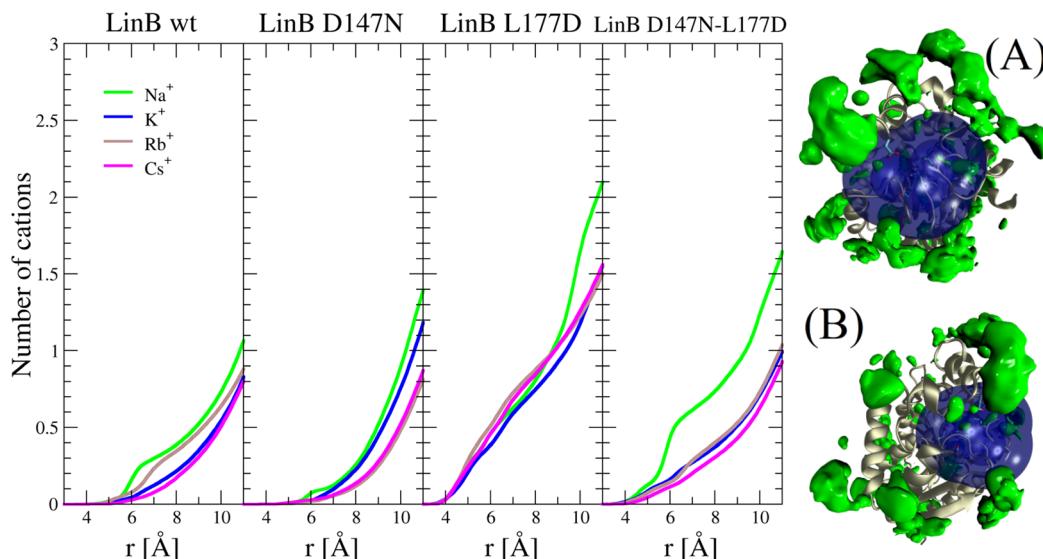


**Figure 6.** Running coordination number of cations to the tunnel mouth for LinB wt, LinB D147N, LinB L177D, and LinB D147N-L177D. The region in which the spatial density is integrated (for 8 Å from the corner opaque-blue points) is visualized in transparent blue on the right for (A) top and (B) for side view.

mouth were counted (Figure S6 in the Supporting Information). This captures a very interesting feature, namely that in most cases cations can reach just the tunnel mouth (at the distance of 12 Å from the nucleophile D108 in the active site), although, in the case of L177D mutation, they can even penetrate into the tunnel and bind around the distance 6 Å, which is not far from the catalytic nucleophile D108. Upon the L177D mutation the tunnel is significantly less hydrophobic, which thus increases the probability of cation penetration into the active site.

**Experiment.** In order to analyze the dependence of the LinB catalytic efficiency on the binding of cations to the hotspot S1, the steady-state kinetics of LinB wt and the mutants LinB D147N and LinB L177D was assayed in aqueous solutions containing 0.5 M of NaCl, KCl, RbCl, or CsCl. The studied single-point mutants carry charge-changing mutation at the hotspot S1, resulting in different cation binding patterns at the tunnel mouth. Unfortunately, the double mutant LinB D147N-L177D could not be characterized experimentally, due to the low protein expression and therefore it is omitted from further analysis.

Before kinetic analysis, we first checked the secondary structures of all the studied enzymes in the presence of alkali chloride salts by circular dichroism spectroscopy to exclude structural changes that would affect enzyme kinetics. No obvious alterations in enzyme conformations were observed (for details see Figure S11 in the Supporting Information). Conversion of the substrate 1-iodohexane to 1-hexanol was then monitored using isothermal titration calorimetry. The kinetics data of LinB wt and LinB D147N were analyzed using a model describing cooperativity and partial substrate inhibition (Figure 7A, and Figure S12 in the Supporting Information).<sup>35</sup>

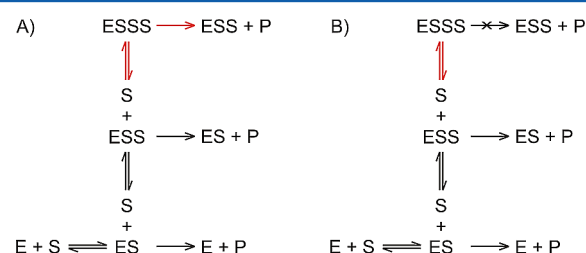


**Figure 7.** Proposed kinetic models explaining the experimental data. (A) Model including cooperativity and partial substrate inhibition. (B) Model including cooperativity and complete substrate inhibition.<sup>35</sup> Red arrows depict the reaction steps affected by inorganic salts.

This type of inhibition results from the formation of a triple-substrate enzyme (ESSS) complex that can generate the product, yet with less efficiency than a double-substrate enzyme (ESS) complex.<sup>36</sup> The partiality of LinB L177D substrate inhibition could not be determined due to the insufficient solubility of the substrate. Thus, all data for this mutant were fitted using an equation describing cooperativity and complete substrate inhibition (Figure 7B, and Figure S12 in the Supporting Information).<sup>35</sup> Simpler mathematical models for enzyme kinetics have also been tested; however, they insufficiently fitted the collected experimental data (for details see Figure S13 in the Supporting Information).

The determined steady-state kinetic parameters are presented in Table 1. Steady-state kinetic parameters were calculated by using the equation describing cooperativity and partial substrate inhibition (eq 3) and the equation describing cooperativity and complete substrate inhibition (eq 4).

$$\frac{\nu}{V_{\text{lim}}} = \frac{[S]^n (1 + b[S]/K_{\text{si}})}{K_{0.5}^n + [S]^n (1 + [S]/K_{\text{si}})} \quad (3)$$

$$\frac{\nu}{V_{\text{lim}}} = \frac{[S]^n}{K_{0.5}^n + [S]^n (1 + [S]/K_{\text{si}})} \quad (4)$$

The mutual comparison of all studied LinB variants revealed that even a point-charge-changing substitution significantly altered the enzyme kinetics. It was shown that substrate inhibition, given by the substrate affinity to the ESS complex or low productivity of ESSS, decreases with increasing negative charge near the access tunnel mouth. According to the strength of substrate inhibition in glycine buffer, the studied enzymes can be ordered as follows: LinB D147N > LinB wt > LinB L177D. Moreover, the comparison of LinB L177D with LinB wt revealed a 3.4-fold decrease in the catalytic constant (Table 1). This result is in agreement with previous observation that a negatively charged residue introduced in the position 177 lowers the catalytic efficiency of LinB.<sup>20</sup>

**Table 1. Steady-State Kinetic Parameters of LinB wt, LinB D147N, and LinB L177D in Buffer and in the Presence of 0.5 M Chloride Salts<sup>a</sup>**

enzyme	solution	$k_{\text{cat}}$ (s <sup>-1</sup> )	$K_{0.5}$ (mM)	$n_H$	$K_{\text{si}}$ (mM)	b
LinB wt	buffer	16.5	0.046	1.3	0.071	0.33
	0.5 M NaCl	16.9	0.050	1.4	0.107	0.10
	0.5 M KCl	16.8	0.047	1.3	0.103	0.12
	0.5 M RbCl	16.7	0.038	1.3	0.085	0.19
	0.5 M CsCl	17.0	0.038	1.3	0.081	0.18
	buffer	16.9	0.040	1.3	0.035	0.02
LinB D147N	0.5 M NaCl	16.9	0.037	1.4	0.035	n.d.
	0.5 M KCl	17.1	0.038	1.4	0.034	n.d.
	0.5 M RbCl	16.7	0.039	1.4	0.039	n.d.
	0.5 M CsCl	17.1	0.038	1.5	0.035	n.d.
LinB L177D	buffer	4.8	0.038	1.3	0.134	n.d.
	0.5 M NaCl	4.0	0.032	1.4	0.474	n.d.
	0.5 M KCl	4.3	0.036	1.3	0.480	n.d.
	0.5 M RbCl	4.4	0.037	1.3	0.443	n.d.
	0.5 M CsCl	4.0	0.032	1.2	0.603	n.d.

<sup>a</sup>All measurements were performed in triplicates at pH 8.6 and 37 °C. All parameters had standard errors of less than 10%. Steady-state kinetic parameters were calculated by using the equation describing cooperativity and partial substrate inhibition (eq 3) and the equation describing cooperativity and complete substrate inhibition (eq 4).  $k_{\text{cat}}$ , catalytic constant;  $k_{\text{cat}} = V_{\text{lim}}/[E]$ ;  $K_{0.5}$ , concentration of substrate at half-maximal velocity;  $K_{\text{si}}$ , substrate inhibition constant;  $n_H$ , Hill coefficient; b, degree of partial inhibition; n.d. = not detected.

The kinetic parameters of all studied enzymes obtained in the presence of alkali chloride salts were compared with those measured in the glycine buffer (100 mM, pH 8.6). The comparison revealed that the addition of alkali chloride salts did not significantly alter the catalytic constant ( $k_{\text{cat}}$ ), the substrate's affinity for the free enzyme ( $K_{0.5}$ ), or the cooperativity ( $n_H$ ) of any of the studied enzymes (Table 1). However, the kinetic constant describing the substrate inhibition of enzymes ( $K_{\text{si}}$ ) was changed in most of the cases, with the exception of LinB D147N. Addition of salts increased the  $K_{\text{si}}$  values of LinB wt and LinB L177D up to 1.5× and 4.5×, respectively (Table 1). For the LinB wt enzyme, the highest increase of  $K_{\text{si}}$  was observed in NaCl. The substrate inhibition for LinB L177D most significantly decreased in CsCl. Thus, these data indicate that substrate affinity to ESS complex is influenced to different extent by individual alkali chloride salts and that this effect becomes stronger with increasing negative charge in the tunnel mouth. As a consequence of reduced substrate inhibition, the reaction rate of LinB L177D was approximately 1.3× higher in the presence of chloride salts than in a pure buffer (Figure 8). Moreover, the level of hyperbolic substrate inhibition (b value), which was observed for LinB wt and LinB D147N, was also salt dependent (Table 1). In the case of LinB wt, the presence of NaCl and KCl led to a 3-fold decrease in the productivity of ESSS complex, whereas RbCl and CsCl reduced this productivity less than twice, resulting in a slight decrease of enzyme reaction rate (Figure 8). Analogously, the addition of alkali chloride salts to the reaction mixture of LinB D147N caused an entire unproductivity of ESSS complex changing the kinetic mechanism from partial to complete substrate inhibition. Nevertheless, in terms of influencing steady-state kinetic parameters of individual enzymes, a strong cationic specificity was not observed.

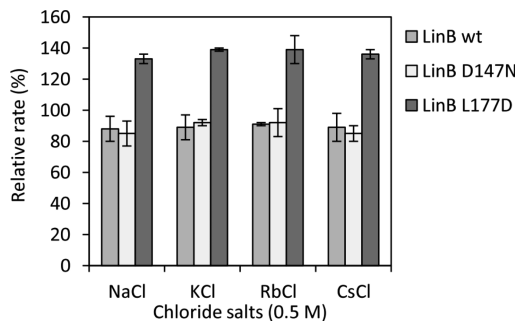


**Figure 8.** Relative reaction rates of LinB wt, LinB D147N, and LinB L177D expressed as a percentage of the reaction rate in glycine buffer ( $\text{pH } 8.6, 37^\circ\text{C}$ ) determined at substrate concentration  $0.15 \text{ mM}$ . The reaction rate of LinB wt, LinB D147N, and LinB L177D in the glycine buffer was  $8.4, 3.4$ , and  $2.1 \text{ mM s}^{-1}$ , respectively.

## CONCLUSIONS

Our combined computational and experimental study of the effects of individual alkali cations on enzymatic activity allows molecular interpretation of the observed Hofmeister ordering. MD simulations provide converged distributions of the four investigated alkali cations around the whole protein. The binding sites for all alkali cations are the same but the strength of binding was different for individual ions. In agreement with our recent study on HIV protease,<sup>15</sup> smaller cations, in particular  $\text{Na}^+$ , bind more strongly to negatively charged surface regions than the larger alkali cations. This result is also consistent with previous observations that interactions of alkali cations with the carboxyl and carbonyl groups at the protein surface correlate with their position in Hofmeister series, i.e.,  $\text{Na}^+ > \text{K}^+ > \text{Rb}^+ > \text{Cs}^+$ .<sup>37</sup>

Based on MD simulation results, two single-point LinB mutants (LinB D147N and LinB L177D), exhibiting different cationic binding at the tunnel mouth, were constructed. The steady-state kinetic analysis of all LinB variants with a substrate 1-iodohexane showed that the enzymatic reaction did not follow a simple Michaelis–Menten kinetics. Instead, the velocity data had to be fitted by a more complex kinetic scheme, including also complexes of the enzyme with two or three substrate molecules. Interestingly, the population of unproductive ESSS complexes was enhanced when a negatively charged aspartate (D147) at the tunnel mouth was mutated to a neutral asparagine (N147), while the mutation of a nearby neutral leucine (L177) to an aspartate (D177) reduced the substrate binding to the ESS complex. This clearly implies involvement of the tunnel mouth in the binding of the third substrate molecule to the enzyme, leading to substrate inhibition. The assumption was further supported by the results of the kinetic measurement in the presence of inorganic salts, showing the cation-specific effect on the substrate inhibition of the studied LinB variants. In agreement with cationic affinities to the LinB wt tunnel mouth, both formation and productivity of ESSS complexes were inhibited more strongly by  $\text{Na}^+$  and  $\text{K}^+$  than  $\text{Rb}^+$  and  $\text{Cs}^+$ . Importantly, this cation specific effect was modified by charge-changing mutations at the tunnel mouth, altering the cationic binding. The extent of the cationic influence on the formation of ESSS was decreased by introduction of neutral residue instead of negative one, and vice versa, increased by introduction of negatively charged residue, although with a weaker cationic specificity. It is important to note that a lower cationic

specificity was observed in this case not only experimentally but also computationally. The substrate inhibition of the mutant LinB L177D in the presence of chloride salts was approximately 7 times lower than that of LinB wt in the glycine buffer. Such suppression of substrate inhibition implies increased catalytic efficiency of the enzyme at high substrate concentration, which is required mainly in industrial biocatalytic processes.

In conclusion, our integrated experimental and computational study attempts to rationalize how the specific cationic effects on LinB activity are connected with the attraction of individual alkali cations to the enzyme tunnel mouth. The obtained results allow us to formulate the following conclusions:

1. The effects of alkali cations on enzyme catalytic parameters were observable and specific, but relatively weak. This is likely due to the fact that the cations interact with the surface of the protein including the tunnel mouth, but do not penetrate directly inside the negatively charged active site. Therefore, cations cannot directly affect the residues involved in the catalytic activity.

2. The impact of point mutations at the tunnel mouth on cation-specific effects on enzymatic catalysis, together with mutation-induced changes in substrate–enzyme binding, affirm the significance of the tunnel residues, as has been proposed previously. Tunnels represent very important structural feature of HLDs, which plays a crucial role in both substrate binding and product release.<sup>22</sup> Engineering of charges at the tunnel openings in combination with addition of salts to the reaction mixture is thus a potential strategy for removal of substrate inhibition at high substrate concentrations.

3. Combination of the facts that the action of alkali cations is outside the active site and that a relatively complex kinetic scheme has to be invoked to fit the experimental data warns against oversimplified interpretations. The main observation of this work, the fact that cations affects enzyme activity by modulation of the substrate inhibition, opens up a possibility for future research; namely the effect of cations on the catalysis of substrates lacking the substrate inhibition may be explored.<sup>38</sup>

## ASSOCIATED CONTENT

### Supporting Information

Further details about MD calculations, computational results for LinB with singly protonated catalytic histidine H272, CD spectra in chloride salts of LinB WT and LinB mutants, and steady-state kinetic data. This material is available free of charge via the Internet at <http://pubs.acs.org>.

## AUTHOR INFORMATION

### Corresponding Author

\*E-mail: radka@chemi.muni.cz (R.C.); jan.heyda@helmholtz-berlin.de (J.H.). Tel.: +420549493567 (R.C.); +4930806242783 (J.H.).

### Present Address

<sup>†</sup>F-ISFM Soft Matter and Functional Materials, Helmholtz-Zentrum Berlin für Materialien und Energie, Hahn-Meitner-Platz 1, 14109 Berlin, Germany.

### Notes

The authors declare no competing financial interest.

## ACKNOWLEDGMENTS

Support to P.J. from the Czech Science Foundation (grant no. P208/12/G016) and the Academy of Sciences (Praemium

Academie award) is gratefully acknowledged. V.S., R.C., and J.D. acknowledge support from the Czech Science Foundation (grant no. P207/12/0775) and the European Regional Development Fund (CZ.1.05/1.1.00/02.0123). J.P. thanks the International Max-Planck Research School for support.

## ■ REFERENCES

- (1) Lo Nostro, P.; Ninham, B. W. Hofmeister Phenomena: An Update on Ion Specificity in Biology. *Chem. Rev.* **2012**, *112*, 2286–2322.
- (2) Hofmeister, F. Zur Lehre von der Wirkung der Salze. *Arch. Exp. Pathol. Pharmakol. (Leipzig)* **1888**, *24*, 247–260.
- (3) Kunz, W.; Henle, J.; Ninham, B. W. “Zur Lehre von der Wirkung der Salze” (About the Science of the Effect of Salts): Franz Hofmeister’s Historical Papers. *Curr. Opin. Colloid Interface Sci.* **2004**, *9* (1–2), 19–37.
- (4) Kunz, W.; Lo Nostro, P.; Ninham, B. W. The Present State of Affairs with Hofmeister Effects. *Curr. Opin. Colloid Interface Sci.* **2004**, *9* (1–2), 1–18.
- (5) Rembert, K. B.; Paterova, J.; Heyda, J.; Hilty, C.; Jungwirth, P.; Cremer, P. S. Molecular Mechanisms of Ion-Specific Effects on Proteins. *J. Am. Chem. Soc.* **2012**, *134*, 10039–10046.
- (6) Zhang, Y. J.; Cremer, P. S. Interactions between Macromolecules and Ions: the Hofmeister Series. *Curr. Opin. Chem. Biol.* **2006**, *10* (6), 658–663.
- (7) Dempsey, C. E.; Mason, P. E.; Jungwirth, P. Complex Ion Effects on Polypeptide Conformational Stability: Chloride and Sulfate Salts of Guanidinium and Tetrapropylammonium. *J. Am. Chem. Soc.* **2011**, *133*, 7300–7303.
- (8) Mason, P. E.; Dempsey, C. E.; Vrbka, L.; Heyda, J.; Brady, J. W.; Jungwirth, P. Specificity of Ion-Protein Interactions: Complementary and Competitive Effects of Tetrapropylammonium, Guanidinium, Sulfate, and Chloride Ions. *J. Phys. Chem. B* **2009**, *113*, 3227–3234.
- (9) Collins, K. D.; Neilson, G. W.; Enderby, J. E. Ions in Water: Characterizing the Forces that Control Chemical Processes and Biological Structure. *Biophys. Chem.* **2007**, *128* (2–3), 95–104.
- (10) Yang, Z.; Liu, X. J.; Chen, C.; Halling, P. J. Hofmeister Effects on Activity and Stability of Alkaline Phosphatase. *Biochim. Biophys. Acta: Proteins Proteomics* **2010**, *1804* (4), 821–828.
- (11) Darnell, J. E.; Lodish, H. F.; Baltimore, D. *Molecular Cell Biology*; Scientific American Books: New York, 1990.
- (12) Collins, K. D. Charge Density-dependent Strength of Hydration and Biological Structure. *Biophys. J.* **1997**, *72* (1), 65–76.
- (13) Wondrak, E. M.; Louis, J. M.; Oroszlan, S. The Effect of Salt on the Michaelis Menten Constant of the HIV-1 Protease correlates with the Hofmeister Series. *FEBS Lett.* **1991**, *280* (2), 344–346.
- (14) Heyda, J.; Pokorna, J.; Vrbka, L.; Vacha, R.; Jagoda-Cwiklik, B.; Konvalinka, J.; Jungwirth, P.; Vondrasek, J. Ion Specific Effects of Sodium and Potassium on the Catalytic Activity of HIV-1 Protease. *Phys. Chem. Chem. Phys.* **2009**, *11* (35), 7599–7604.
- (15) Pokorna, J.; Heyda, J.; Konvalinka, J. Ion Specific Effects of Alkali Cations on the Catalytic Activity of HIV Protease. *Faraday Discuss.* **2013**, *160*, 359–370.
- (16) Friedman, R. Ions and the Protein Surface Revisited: Extensive Molecular Dynamics Simulations and Analysis of Protein Structures in Alkali-Chloride Solutions. *J. Phys. Chem. B* **2011**, *115*, 9213–9223.
- (17) Damborsky, J.; Rorije, E.; Jesenska, A.; Nagata, Y.; Klopman, G.; Peijnenburg, W. Structure-specificity relationships for haloalkane dehalogenases. *Environ. Toxicol. Chem.* **2001**, *20* (12), 2681–2689.
- (18) Verschueren, K. H. G.; Seljee, F.; Rozeboom, H. J.; Kalk, K. H.; Dijkstra, B. W. Crystallographic Analysis of the Catalytic Mechanism of Haloalkane Dehalogenase. *Nature* **1993**, *363* (6431), 693–698.
- (19) Chovancova, E.; Kosinski, J.; Bujnicki, J. M.; Damborsky, J. Phylogenetic Analysis of Haloalkane Dehalogenases. *Proteins: Struct. Funct. Bioinf.* **2007**, *67* (2), 305–316.
- (20) Chaloupkova, R.; Sykorova, J.; Prokop, Z.; Jesenska, A.; Monincovaa, M.; Pavlova, M.; Tsuda, M.; Nagata, Y.; Damborsky, J. Modification of Activity and Specificity of Haloalkane Dehalogenase from *Sphingomonas Paucimobilis* UT26 by Engineering of its Entrance Tunnel. *J. Biol. Chem.* **2003**, *278* (52), 52622–52628.
- (21) Pavlova, M.; Klvana, M.; Prokop, Z.; Chaloupkova, R.; Banas, P.; Otyepka, M.; Wade, R. C.; Tsuda, M.; Nagata, Y.; Damborsky, J. Redesigning Dehalogenase Access Tunnels as a Strategy for Degrading an Anthropogenic Substrate. *Nat. Chem. Biol.* **2009**, *5* (10), 727–733.
- (22) Marek, J.; Vevodova, J.; Smatanova, I. K.; Nagata, Y.; Svensson, L. A.; Newman, J.; Takagi, M.; Damborsky, J. Crystal Structure of the Haloalkane Dehalogenase from *Sphingomonas Paucimobilis* UT26. *Biochemistry* **2000**, *39*, 14082–14086.
- (23) Oakley, A. J.; Klvana, M.; Otyepka, M.; Nagata, Y.; Wilce, M. C. J.; Damborsky, J. Crystal Structure of Haloalkane Dehalogenase LinB from *Sphingomonas Paucimobilis* UT26 at 0.95 Ångstrom Resolution: Dynamics of Catalytic Residues. *Biochemistry* **2004**, *43*, 870–878.
- (24) Jurkiewicz, P.; Cwiklik, L.; Vojtiskova, A.; Jungwirth, P.; Hof, M. Structure, Dynamics, and Hydration of POPC/POPS Bilayers Suspended in NaCl, KCl, and CsCl Solutions. *Biochim. Biophys. Acta: Biomembr.* **2012**, *1818* (3), 609–616.
- (25) Duan, Y.; Wu, C.; Chowdhury, S.; Lee, M. C.; Xiong, G. M.; Zhang, W.; Yang, R.; Cieplak, P.; Luo, R.; Lee, T.; Caldwell, J.; Wang, J. M.; Kollman, P. A Point-Charge Force Field for Molecular Mechanics Simulations of Proteins Based on Condensed-Phase Quantum Mechanical Calculations. *J. Comput. Chem.* **2003**, *24* (16), 1999–2012.
- (26) Berendsen, H. J. C.; Grigera, J. R.; Straatsma, T. P. The Missing Term in Effective Pair Potentials. *J. Phys. Chem.* **1987**, *91*, 6269–6271.
- (27) Case, D. A.; Darden, T. A.; Cheatham, III, T. E.; Simmerling, C. L.; Wang, J.; Duke, R. E.; Luo, R.; Walker, R. C.; Zhang, W.; Merz, K. M.; Roberts, B.; et al. AMBER 11; University of California: San Francisco, 2010.
- (28) Heyda, J.; Kozisek, M.; Bednarova, L.; Thompson, G.; Konvalinka, J.; Vondrasek, J.; Jungwirth, P. Urea and Guanidinium Induced Denaturation of a Trp-Cage Miniprotein. *J. Phys. Chem. B* **2011**, *115*, 8910–8924.
- (29) Ryckaert, J. P.; Ciccotti, G.; Berendsen, H. J. C. Numerical-Integration of Cartesian Equations of Motion of a System with Constraints - Molecular-Dynamics of N-Alkanes. *J. Comput. Phys.* **1977**, *23* (3), 327–341.
- (30) Essmann, U.; Perera, L.; Berkowitz, M. L.; Darden, T.; Lee, H.; Pedersen, L. G. A Smooth Particle Mesh Ewald Method. *J. Chem. Phys.* **1995**, *103* (19), 8577–8593.
- (31) Berendsen, H. J. C.; Postma, J. P. M.; Vangunsteren, W. F.; Dinola, A.; Haak, J. R. Molecular-Dynamics with Coupling to an External Bath. *J. Chem. Phys.* **1984**, *81* (8), 3684–3690.
- (32) Willard, A. P.; Chandler, D. Instantaneous Liquid Interfaces. *J. Phys. Chem. B* **2010**, *114*, 1954–1958.
- (33) Nagata, Y.; Hynkova, K.; Damborsky, J.; Takagi, M. Construction and Characterization of Histidine-Tagged Haloalkane Dehalogenase (LinB) of a New Substrate Class from a Gamma-Hexachlorocyclohexane-Degrading Bacterium, *Sphingomonas Paucimobilis* UT26. *Protein Expression Purif.* **1999**, *17* (2), 299–304.
- (34) Jungwirth, P. Ions at Aqueous Interfaces. *Faraday Discuss.* **2009**, *141*, 9–30.
- (35) Segel, I. H. *Enzyme Kinetics: Behavior and Analysis of Rapid Equilibrium and Steady-State Enzyme Systems*; Wiley-Interscience: New York, 1993.
- (36) Whiteley, C. G. Enzyme Kinetics: Partial and Complete Competitive Inhibition. *Biochem. Educ.* **1997**, *25* (3), 144–146.
- (37) Vrbka, L.; Vondrasek, J.; Jagoda-Cwiklik, B.; Vacha, R.; Jungwirth, P. Quantification and Rationalization of the Higher Affinity of Sodium over Potassium to Protein Surfaces. *Proc. Natl. Acad. Sci. U.S.A.* **2006**, *103* (42), 15440–15444.
- (38) Prokop, Z.; Monincova, M.; Chaloupkova, R.; Klvana, M.; Nagata, Y.; Janssen, D. B.; Damborsky, J. Catalytic Mechanism of the Haloalkane Dehalogenase LinB from *Sphingomonas Paucimobilis* UT26. *J. Biol. Chem.* **2003**, *278* (46), 45094–45100.